Electrochimica Acta 301 (2019) 47–54

Contents lists available at ScienceDirect

Electrochimica Acta

journal homepage: www.elsevier.com/locate/electacta

Temperature effect on crystallinity and chemical states of nickel hydroxide as alternative superior catalyst for urea electrooxidation

Qiuping Gan [a, 1], Xiaoyang Cheng [a, 1], Judan Chen [a], Dongsheng Wang [a], Benzhi Wang [a], Jianniao Tian [a, **], Tayirjan Taylor Isimjan [b, ***], Xiulin Yang [a, *]

[a] Key Laboratory for the Chemistry and Molecular Engineering of Medicinal Resources (Ministry of Education of China), College of Chemistry and Pharmacy, Guangxi Normal University, Guilin, 541004, PR China
[b] Saudi Arabia Basic Industries on (SABIC) at King Abdullah University of Science and Technology (KAUST), Saudi Arabia

ARTICLE INFO

Article history:
Received 17 December 2018
Accepted 26 January 2019
Available online 29 January 2019

Keywords:
Nickel hydroxide
Temperature effect
Crystal structure
Urea electrooxidation
Electrocatalysis

ABSTRACT

Developing a highly efficient and stable catalyst, composited by inexpensive, earth-abundant and non-toxic materials, is the critical issue for electrochemical urea oxidation. Among the all other physical parameters, the reaction temperature plays the key role in catalyst performance. Herein, we have studied the effect of temperatures on the synthesis of nickel hydroxide-carbon nanotubes composites via a facile hydrothermal method and the catalytic performance towards urea electro-oxidation in detail. Our studies indicate that the higher temperature enhances the crystallinity of β-$Ni(OH)_2$ species. Furthermore, the Ni(III) species in $Ni(OH)_2$-CNTs composites show an optimal point upon the changes of the reaction temperature, and the highest Ni(III) content appears at 80 °C of β-$Ni(OH)_2$-CNTs. Meanwhile, electrochemical studies show that the electrochemically active surface areas (ESA) of the optimized β-$Ni(OH)_2$-CNTs (80 °C, 95.6 $m^2 g^{-1}$) catalyst is 4.51- and 2.76-fold higher than that of β-$Ni(OH)_2$-CNTs synthesized at 20 and 140 °C, respectively. The higher ESA of β-$Ni(OH)_2$-CNTs (80 °C) also accompanies a superior electrochemical urea oxidation with a peak current density of 98.5 mA cm^{-2}, significantly higher than all the other studied catalysts. Additionally, the optimal β-$Ni(OH)_2$-CNTs (80 °C) also demonstrates the highest initial and limiting current densities after uninterrupted long-term operation. These excellent performance of β-$Ni(OH)_2$-CNTs (80 °C) catalyst indicates the positive effect of Ni(III) content which provides more catalytically active species along with the unique lamellar structures of CNTs as the support to facilitate electron/mass transfer and gas emission.

© 2019 Elsevier Ltd. All rights reserved.

1. Introduction

With the increase in energy demand and environmental pollution, the development of renewable energy (wind, solar, biomass, etc.) has gradually become the main theme in replacing fossil fuel [1,2]. Hydrogen, as a fuel with high specific energy density, has captured a lot of attentions due to its clean and sustainable features [3,4]. With the rising enthusiasm on hydrogen energy research, urea electrooxidation has evolved into a hotspot because the reaction can provide fuel energy directly at the anode, meanwhile hydrogen can be released at the cathode during the electrolysis [5,6]. Studies have found that the urea catalytic system consumes less electrical energy than the water electrolysis in the case of producing the same hydrogen [7]. In addition, the consumption of urea is of great significance in eliminating environmental pollution because there is an approximately 2–2.5% of urea discharged in wastewater from various industrial streams [8]. Most of studies found that noble metal catalysts such as Ru-based composites and platinum group metals can improve the catalytic performance of urea oxidation [9,10]. Nevertheless, high cost and scarcity limit their large-scale applications. Therefore, searching low-cost and earth–abundant catalysts to replace the precious metal catalysts for urea electrooxidation is still an urgent problem until now.

Previous studies have shown that non-precious metals also have catalytic performance for urea electrooxidation, such as Ni-M double hydroxides on carbon fiber and Ni foam [11], nickel nanowire arrays on polycarbonate [12], nickel manganese oxide [13],

* Corresponding author.
** Corresponding author.;
*** Corresponding author.
E-mail addresses: birdtjn@sina.com (J. Tian), isimjant@sabic.com (T.T. Isimjan), xiulin.yang@kaust.edu.sa (X. Yang).
[1] These authors contributed equally.

https://doi.org/10.1016/j.electacta.2019.01.150
0013-4686/© 2019 Elsevier Ltd. All rights reserved.

porous Ni_3N nanosheet array on carbon cloth [14], carbon-encapsulated nickel-iron [15], CoS_2 nanoneedle array on Ti mesh [16], multi-layers graphene/nickel [6], sodium nickel fluoride on carbon nanotubes [17], mesoporous nickel phosphide [18], Ni-decorated graphene sheets [19], mesoporous $NiCo_2O_4$ nanosheets [20], NiO-Fe_2O_3 based graphene aerogel [21], hierarchical coral-like Ni-Mo sulfides on Ti mesh [22], three-dimensional MnO_2/$MnCo_2O_4$/Ni [23], two-dimensional metal-organic framework [24], *etc*. Among them, nickel-based catalysts has been extensively explored, but there are still many shortages on catalytic activity, stability, mechanism analysis, *etc*. To further explore and clarify reaction mechanism, many $Ni(OH)_2$-based catalysts are investigated, *e.g.*, exfoliated $Ni(OH)_2$ nanosheets [25], $Ni(OH)_2$ nanoflakes [26], Mn-incorporated $Ni(OH)_2$-carbon fiber [27], carbon nanotube twined α-$Ni(OH)_2$ microspheres [28], S-doped $Ni(OH)_2$ [29], *etc*. However, since the crystallinity and microstructure of $Ni(OH)_2$ are greatly affected by various synthetic factors, the catalytic performance of the prepared materials show great differences [30]. Although the reaction temperature plays the key role in catalyst performance, until now, there is little literature reported to reveal the effect of reaction temperature on the electrocatalytic performance of urea oxidation catalysts. On the other hand, the catalyst supports also have great effect in catalysis performance, *e.g.*, carbon cloth, carbon paper, graphene, nickel foam, CNTs, *etc*. [31–33], in which one-dimensional CNTs has attracted widespread attention due to high surface area, high conductivity, good tensile performance, *etc*. [34].

Herein, we represent a simple one-step hydrothermal method to synthesize a series of $Ni(OH)_2$-CNTs composites with lamellar structures under different reaction temperatures, where the β-phase of $Ni(OH)_2$-CNTs are prepared in the range of 20–140 °C. The study found that the crystallinity of β-$Ni(OH)_2$-CNTs can be feasibly altered by adjusting the reaction temperatures. Various characterization techniques are adopted to explore the crystal structures, morphologies, elemental mappings and chemical states, such as X-ray powder diffraction, scanning electron microscopy, transmission electron microscopy, Raman spectrum and X-ray photoelectron spectroscopy. Electrochemical studies found that the β-$Ni(OH)_2$-CNTs catalyst synthesized at 80 °C exhibits the largest electrochemically active surface area (95.6 $m^2\,g^{-1}$), the highest catalytic activity (98.5 mA cm^{-2}) and long-term stability for urea electro-oxidation. The superior catalytic performance are contributed to the synergistic effect of high content of Ni(III) species on the unique lamellar structured CNTs as the support for β-$Ni(OH)_2$-CNTs composite, and the detailed study is discussed below.

2. Experimental

2.1. Materials

Nickel nitrate hexahydrate ($Ni(NO_3)_2{\cdot}6H_2O$), potassium hydroxide (KOH), sulfuric acid (H_2SO_4), anhydrous ethanol (C_2H_5OH), chloroplatinic acid (H_2PtCl_6) and sodium borohydride ($NaBH_4$) were purchased from commercial chemical company. All the reagents were analytical reagent and used without further purification. Vulcan XC-72R and Carbon nanotubes (CNTs) were purchased from United States Cabot Corporation. Nafion solution (*ca*. 5%) was purchased from Alfa Aesar.

2.2. Synthesis of β-Ni(OH)$_2$-CNTs

The series of β-$Ni(OH)_2$-CNTs was synthesized by a facile hydrothermal reaction, and the specific experiment process was described as follows, where 0.2907 g $Ni(NO_3)_2{\cdot}6H_2O$ (~1.0 mmol) and 100 mg nanotubes (CNTs) were initially put into 10 mL DI-water in a round-bottomed flask. After continuously stirring for 30 min, 10 mL of 2 mM KOH solution was added and sonicated for another 30 min. In order to obtain the composites with different crystal phases and crystallinity, the above-mentioned flasks containing the mixture were placed in a preheated silicone oil bath at different temperatures in the range of 20–140 °C with continuously stirring for 5 h. After cooling down to room temperature, the resulted mixtures were centrifuged, rinsed by abundant water/ethanol, and freeze-dried for overnight. The obtained products were labeled as β-$Ni(OH)_2$-CNTs (20, 40, 60, 80, 100, 120 or 140 °C) according to the reaction temperatures and the subsequent chemical analysis.

For better comparison, the pure β-$Ni(OH)_2$ (80 °C) was prepared by similar experimental process except not adding CNTs. The sample of β-$Ni(OH)_2$+CNTs (80 °C) was synthesized by directly physical mixing methods.

Pt/C (20 wt% Pt) was prepared by a facile direct reduction method, in which a certain amount of H_2PtCl_6 and Vulcan XC-72R were ultrasonically dispersed in a beaker containing 20 mL H_2O. Thirty-minutes later, 10 mL of 5 mg mL^{-1} $NaBH_4$ solution was slowly added dropwise into the above solution under vigorously stirring condition. Two-hours later, the products were collected by centrifugation, washed by abundant ethanol/H_2O and freeze-dried in vacuum box at 60 °C for 12 h.

2.3. Characterization

The morphologies and microstructures of the catalysts were characterized by scanning electron microscopy (SEM, FEI Quanta 200 FEG) with X-ray energy dispersive spectrometer (EDS) and transmission electron microscopy (TEM, JEM-2100F). The crystalline information of catalysts were analyzed by X-ray powder diffraction (XRD, Rigaku D/Max 2500 V/PC) with a sweep speed for 2.0° min^{-1}. Raman spectra (Invia, Renishaw) were used to study the electronic structure of the samples. The X-ray photoelectron spectroscopy (XPS, JPS-9010 Mg Kα) was used to analyze the chemical states of different elements. The binding energy was calibrated based on the 284.8 eV C 1s peak and with a standard deviation of approximately ±0.05 eV.

2.4. Electrochemical measurements

All electrochemical measurements were carried out in a standard three-electrode cell using Bio-logic VMP3 working station at room temperature. Glassy carbon electrode (GCE), Pt foil and saturated calomel electrode (SCE) were used as the working, counter and reference electrodes, respectively. The glassy carbon electrode was polished with aluminum powder and then cleaned in sulfuric acid, ethanol and water subsequently for three times before use. The working electrode were prepared as follows: 4.0 mg catalyst was ultrasonically dispersed into mixed solution containing 768 μL H_2O, 200 μL ethanol and 32 μL of 0.5 wt% Nafion solution for 30 min to form a uniform solution. Then, 10 μL catalyst inks was pipetted onto the GCE surface ($\phi = 3$ mm and automatically drying in the air at room temperature. The loading of catalyst on GCE is *ca*. 0.57 mg cm^{-2}. The cyclic voltammograms (CV) measurements were recorded at a potential range from 0.0 to 0.8 V (vs. SCE) with a scan rate of 50 mV s^{-1} in N_2-saturated 1.0 M KOH with and without 0.33 M urea electrolyte. The stability of urea electro-oxidation was performed by chronoamperometry at constant potential 0.45 V (vs. SCE) for continuous 2.0 h in 1.0 M KOH +0.33 M urea solution. All the electrochemical tests were performed at room temperature (25 ± 1 °C).

3. Results and discussion

3.1. Crystal structure analysis

The crystal structures and crystallinity of the synthesized series of $Ni(OH)_2$ with and without coexisting CNTs are initially investigated. Fig. 1 shows that the crystal structures of $Ni(OH)_2$ synthesized at 20, 80 and 140 °C are perfectly consistent with the standard model of hexagonal β-$Ni(OH)_2$ (JCPDS: 14–0117) [35], and the distinct peaks at 19.3, 33.1, 38.4, 52.0, 59.1, 62.6, 69.3, 72.7 and 82.6° are corresponding to (001), (100), (101), (102), (110), (111), (200), (201) and (202) crystal planes, respectively [36]. After incorporation of CNTs, there are two additional peaks appearance at 25.8 and 43.5° corresponding to (002) and (101) crystal planes of CNTs, respectively [37]. In addition, one should note that the diffraction peaks position of NiOOH are very close to these of β-$Ni(OH)_2$ as shown in Fig. S1, so the both species may coexist in the samples. Moreover, we can observe that the β-$Ni(OH)_2$ synthesized at low temperatures (*e.g.*, 20 and 80 °C) exhibit a wider half-width and weaker peak intensity compared to the sample prepared at high temperature (*e.g.*, 140 °C), indicating that β-$Ni(OH)_2$ synthesized at low temperatures have a smaller crystallite sizes, and low crystallinity which increases gradually with increasing the reaction temperatures [38].

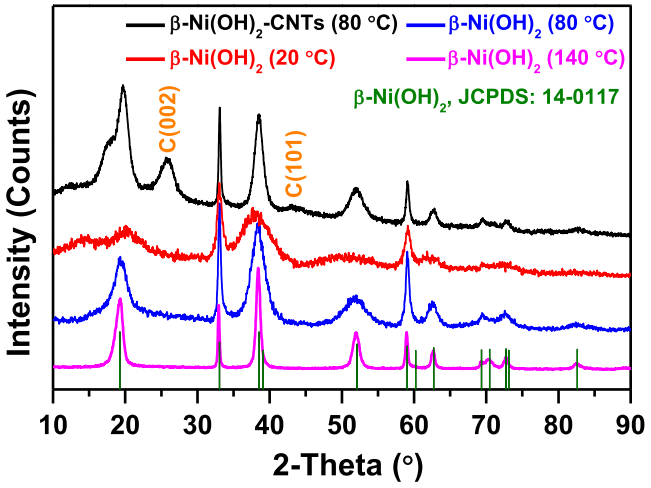

Fig. 1. X-ray diffraction (XRD) patterns of β-$Ni(OH)_2$ with and without addition of CNTs synthesized at 20, 80 and 140 °C, respectively.

3.2. Morphology and microstructure analysis

The morphologies and compositions of $Ni(OH)_2$-CNTs synthesized at 20, 80 and 140 °C are further explored by SEM images and EDS mappings. The SEM image of β-$Ni(OH)_2$-CNTs (20 °C) is composited of continuous wavy-like structures (Fig. 2a). The β-$Ni(OH)_2$-CNTs (80 °C) exhibits a layered structures with the fish scales diameter of around 2 μm (Fig. 2b–c). As for comparison, we also carried out the experiment using water bath instead of an oil bath. The resulted sample in a water bath shows a honeycomb structure (Fig. S2) due to the no uniform heating. Notably, the high surface roughness of β-$Ni(OH)_2$-CNTs (80 °C) compare to that of the β-$Ni(OH)_2$-CNTs (20 °C) results larger surface area that is beneficial for facilitating mass transfer as well as gas emission through the layered spacing. When the reaction temperature reaches to 140 °C (Fig. 2d–e), the layered β-$Ni(OH)_2$-CNTs becomes much thicker and larger than that of prepared at 80 °C together with the narrower layered spacing as a result of the higher crystallinity as observed in XRD patterns. Additionally, the EDS mappings indicate that the Ni, O, and C elements are all uniformly distributed on the surface of the β-$Ni(OH)_2$-CNTs (80 °C).

The microstructures of the synthesized β-$Ni(OH)_2$-CNTs (80 °C) are also observed by TEM. The β-$Ni(OH)_2$ species exists in the form of layered structures and evenly intertwined with CNTs in the composites (Fig. 3a) which enhances the electrical conductivity of the composite. High-resolution TEM image (Fig. 3b) shows two

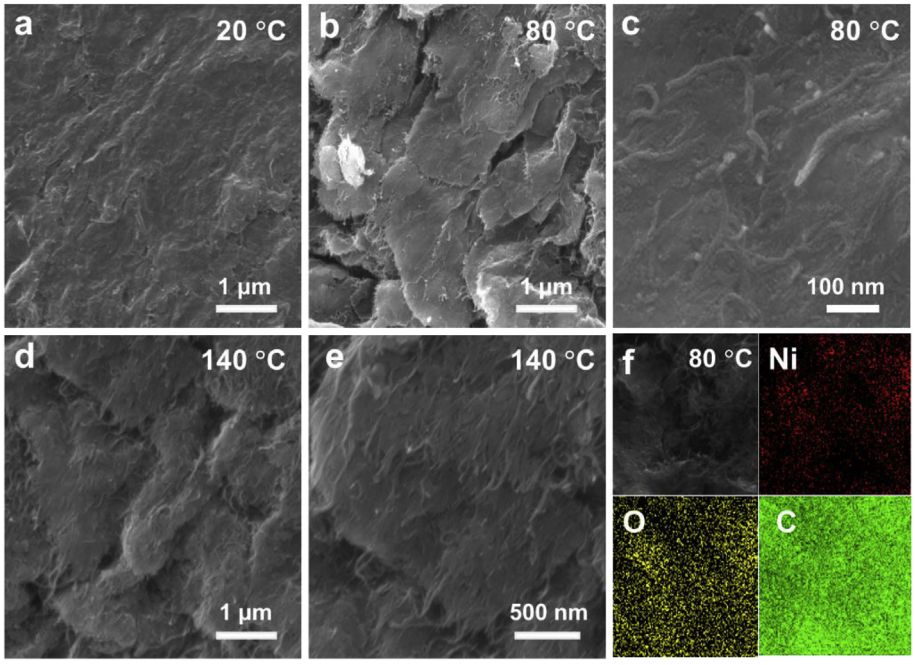

Fig. 2. Scanning electron microscopy (SEM) images of (a) β-$Ni(OH)_2$-CNTs (20 °C), (b–c) β-$Ni(OH)_2$-CNTs (80 °C) and (d–e) β-$Ni(OH)_2$-CNTs (140 °C). (f) Energy-dispersive X-ray spectroscopy (EDS) mappings of β-$Ni(OH)_2$-CNTs (80 °C) with Ni, O, C elements.

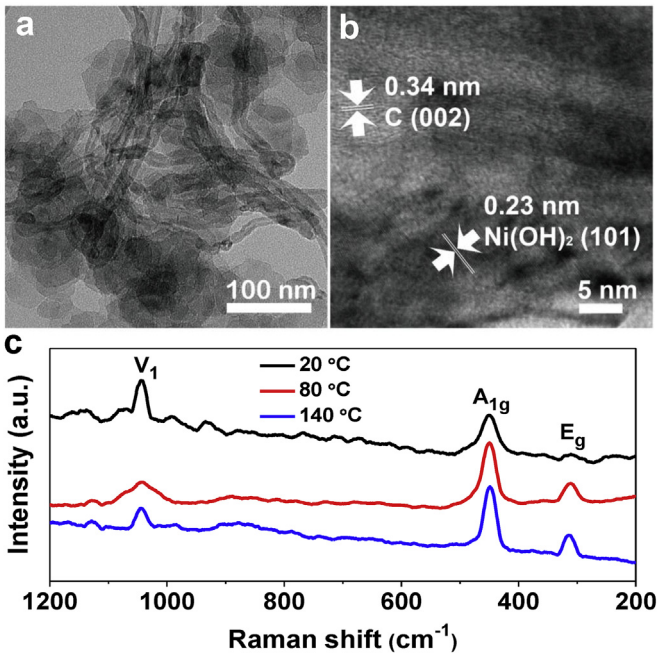

Fig. 3. (a) Transmission electron microscopy (TEM) and (b) high-resolution TEM images of β-Ni(OH)$_2$-CNTs (80 °C). (c) Raman spectrum of β-Ni(OH)$_2$ prepared at 20, 80 and 140 °C, respectively.

types of clear the lattice spacings for *ca.* 0.23 and 0.34 nm representing (101) facet of β-Ni(OH)$_2$ and (002) facet of graphite, respectively [39,40]. Raman spectrum is also used to distinguish the differences of the pure Ni(OH)$_2$ at various temperatures (Fig. 3c). The β-Ni(OH)$_2$ (20 °C) exhibits two distinctive peaks in the range of 20–200 cm^{-1}, where the signal at 450 cm^{-1} is assigned to the Ni-O stretching (A_{1g}) and the band at 1044 cm^{-1} is originated from the V_1 mode of nitrate ions located in the interlayer space [41]. When the reaction temperatures increase from 20 to 80 and 140 °C, a new peak appears at 312 cm^{-1} corresponding to the E-type vibration mode of the Ni–OH lattice [42]. Notably, the Ni(OH)$_2$ synthesized at 80 °C exhibits a broader peak at 1044 cm^{-1} compare to these of Ni(OH)$_2$ prepared at 20 and 140 °C, indicating wider layered spacings.

3.3. Chemical states analysis

The XPS measurements were performed on the Ni(OH)$_2$-CNTs prepared at 20, 80 and 140 °C to identify each components and chemical states of Ni in Ni(OH)$_2$-CNTs catalysts. The results demonstrate that all the samples are composited by Ni, O and C elements (Fig. S3). As shown in Fig. S4, the high-resolution C 1s spectra of each sample have been convoluted into three peaks at C=C (284.0 eV), C-C (284.8 eV) and C-O (286.0 eV) [43]. As shown in Fig. 4a, the Ni 2p$_{3/2}$ spectra of three samples are split into four peaks with binding energies of 854.5, 855.8, 857.1 and 862.2 eV, which are corresponding to the NiO, Ni(OH)$_2$, NiOOH and satellite peak, respectively [35,44]. The results indicate that the Ni(III) content in β-Ni(OH)$_2$-CNTs (80 °C) is 54.2%, which is significantly higher than these in β-Ni(OH)$_2$-CNTs (20 °C, 9.3%) and β-Ni(OH)$_2$-CNTs (140 °C, 29.5%). Meanwhile, the Ni(III) species in β-Ni(OH)$_2$-CNTs (80 °C) was also confirmed by chemical analysis (Fig. S5). It is well accepted that the higher content of Ni(III) species in the hybrid catalyst is considered to be one of the most important reasons contributing to the high catalytic performance for urea electrooxidation [29]. Moreover, the high-resolution O 1s spectra of the three samples are further analyzed (Fig. 4b), and four types of signals originating from different oxygen species are observed. The peaks with the binding energies at 529.8, 530.9, 532.0 and 533.0 eV could be ascribed to the Ni–O, oxygen vacancies, C–O, and adsorbed H_2O/C=O, respectively [45–47]. In general, the high oxygen vacancies mean more active sites, better electron transport capacity, and optimal adsorption energy thereby resulting higher catalytic performance [48]. Interestingly, the content of O vacancies in the samples decreases gradually with increasing the reaction temperatures. The

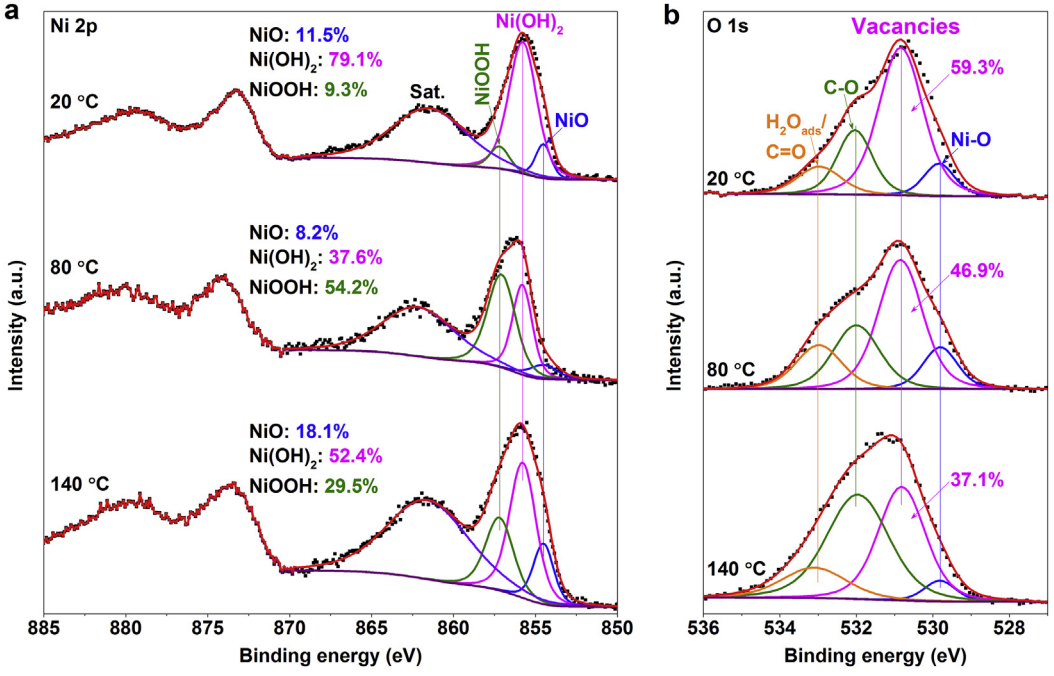

Fig. 4. High-resolution X-ray photoelectron spectroscopy (XPS) of (a) Ni 2p and (b) O 1s regions from β-Ni(OH)$_2$-CNTs (20 °C), β-Ni(OH)$_2$-CNTs (80 °C) and β-Ni(OH)$_2$-CNTs (140 °C).

content of O vacancies in β-Ni(OH)$_2$-CNTs (80 °C) is 46.9%, which is significantly higher than that of the β-Ni(OH)$_2$-CNTs prepared at 140 °C (37.1%), but lower than that of the β-Ni(OH)$_2$ synthesized at 20 °C (59.3%), implying the catalytic performance is outcome of the combined effect of various parameters such as the oxygen vacancies, content of the Ni(III) species and the catalyst support.

3.4. Electrochemically active surface area analysis

The CV curves of Ni(OH)$_2$-CNTs synthesized at different temperatures are investigated in 1.0 M KOH solution to calculate their electrochemically active surface area (ESA) (Fig. 5a). All the samples except CNTs, show a pair of redox peaks in the potential range of 0.0–0.8 V (vs. SCE), where there is an anode peak in the forward scan corresponding to partially oxidized Ni(OH)$_2$ species to NiOOH, and a cathode peak in the backward scan is ascribed to the reversible reduction of the generated NiOOH species to Ni(OH)$_2$ on the catalyst surface [35,49]. Generally, the required reduction charge in the backward scan is used to calculate the ESA, which is normally proportional to the exposed active sites for urea electro-oxidation. The ESA of different catalysts could be evaluated by using the equation of ESA = Q/mq, where Q is the amount of total charge requested to reduce NiOOH to Ni(OH)$_2$, m is the amount of Ni in the hybrid catalysts, and q is 257 μC cm^{-2} for the one electron process in the conversion of NiOOH to Ni(OH)$_2$. As shown in Fig. 5b, we can observe that the ESA values increase with rising the synthetic temperatures from 20 to 80 °C (95.6 m^2 g^{-1}), and then decrease gradually after the synthetic temperatures over 80 °C, indicating that the β-Ni(OH)$_2$-CNTs (80 °C) has the maximum amount of active sites for urea electro-oxidation.

To further explore the influence of synthetic method on ESA, the β-Ni(OH)$_2$+CNTs (80 °C) and Pt/C (20 wt%) are also studied in 1.0 M KOH (Fig. 5c). It is observed that the ESA value of β-Ni(OH)$_2$+CNTs (80 °C) prepared by direct physical mixing method is 34.6 m^2 g^{-1} (Fig. 5d), which is obviously higher than pure β-Ni(OH)$_2$ (80 °C, Fig. S6), but significantly lower than that of the β-Ni(OH)$_2$-CNTs (80 °C) prepared by one-step hydrothermal method, indicating the positive effect of the support as well as the fabrication method on the catalytic performance.

3.5. Electrochemical urea oxidation analysis

In general, the electro-catalytic activity of a catalyst is proportional to its ESA value. Thus, the electro-catalytic activity of β-Ni(OH)$_2$-CNTs (80 °C) together with other control catalysts are further explored in urea electro-oxidation (Fig. 6a and Fig. S7). All the catalysts show a similar onset potential at *ca.* 0.32 V, and the

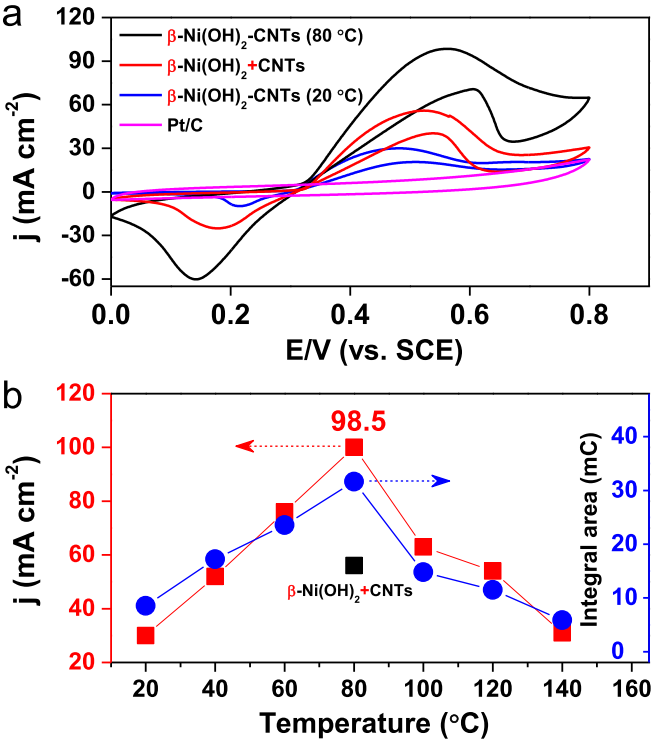

Fig. 6. (a) CV curves of different catalysts in 1.0 M KOH + 0.33 M urea with a scan rate of 50 mV s^{-1}. (b) Summarized forward current densities and integral charges of β-Ni(OH)$_2$-CNTs catalysts synthesized at different temperatures for urea electrooxidation.

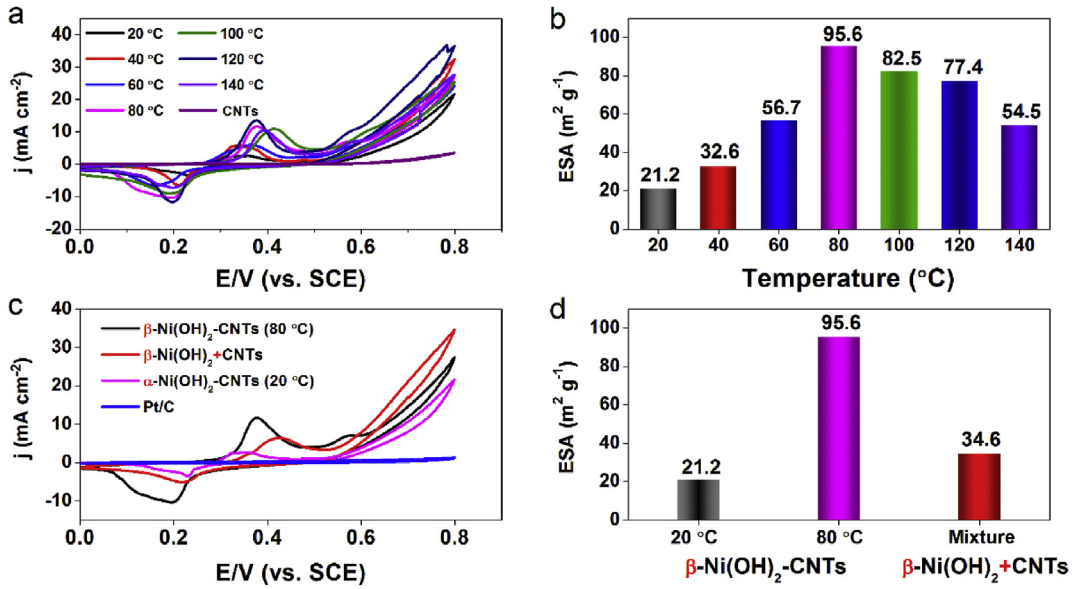

Fig. 5. (a) Cyclic voltammograms (CV) of series Ni(OH)$_2$-CNTs catalysts synthesized at different temperatures operated in 1.0 M KOH with a scan rate of 10 mV s^{-1}, and (b) the corresponding summarized ESA values from a. (c) CV curves of synthesized different control catalysts tested in 1.0 M KOH, and (d) the corresponding summarized ESA values from c.

current densities gradually increase with increasing the applied potentials until the peak potentials. In this process, the $Ni(OH)_2$ species on the catalyst surface will firstly lose one electron to form NiOOH species [$Ni(OH)_2 + OH^- \leftrightarrow NiOOH + H_2O + e^-$] [15]. Subsequently, the generated NiOOH species will adsorb urea molecules and hydroxyl ions from the electrolyte. After enduring a complicated multi-electron transfer process, the urea molecules are eventually oxidized to CO_2, N_2 and H_2O [$CO(NH_2)_2 + 6OH^- \rightarrow CO_2 + N_2 + 5H_2O + 6e^-$] [29]. A slight degradation of catalytic activity after peak potentials and the lower reverse current densities are speculated to be caused by the gas bubbles of the final products (*e.g.*, CO_2, N_2) or the active sites blocking by the reaction intermediates. Furthermore, there is a reduction peak appearance in the reverse scan in the range of 0.32 to 0 V, which is resulted by the reduction of the NiOOH species to $Ni(OH)_2$ species during the forward scan [55]. Combined with these understandings, the total charge of urea oxidation can be expressed as the equation of $\Delta Q_{urea} = Q_{anode} - Q_{cathode}$ [18], where Q_{anode} is the total amount of charge consumed during forward oxidation, and $Q_{cathode}$ is the amount of charge required for the restoration of NiOOH to $Ni(OH)_2$. The summary of the forward peak current densities and the charge required for urea oxidation (ΔQ_{urea}) by β-$Ni(OH)_2$-CNTs (80 °C) and various control catalysts are shown in Fig. 6b and Fig. S8. The results indicate that the forward peak current densities and ΔQ_{urea} exhibit a similar trends on the β-$Ni(OH)_2$-CNTs catalysts synthesized at different temperatures for urea electro-oxidation. However, the β-$Ni(OH)_2$-CNTs (80 °C) shows the highest the forward peak current density (98.5 mA cm^{-2}) and ΔQ_{urea} (31.64 mC), which is 1.76- and 8.01-fold higher than that of β-$Ni(OH)_2$ + CNTs (80 °C, 55.9 mA cm^{-2}) and pure β-$Ni(OH)_2$ (80 °C, 12.3 mA cm^{-2}), consistent with the changes of ESA values as discussed above. Notably, the optimal β-$Ni(OH)_2$-CNTs (80 °C) catalyst is also better than most previously reported urea electrocatalysts in terms of onset potentials, peak current densities and so on (Table 1).

The stability of β-$Ni(OH)_2$-CNTs (80 °C) together with the control catalysts are evaluated by chronoamperometry at a fixed potential of 0.45 V (vs. SCE) and uninterrupted multi-cycles CV method in 1.0 M KOH +0.33 M urea solution. As shown in Fig. 7, the β-$Ni(OH)_2$-CNTs (80 °C) catalyst demonstrates the highest initial current density and limiting current density compared to other control catalysts. The initial high current density is due to the relatively high urea concentration adsorbed on the catalyst surface, and the subsequent slow decay is due to the produced gas bubbles (*e.g.*, CO_2, N_2) or the active sites blockage by the reaction intermediate products [28]. After continuous running for 7200 s, the limiting current density of β-$Ni(OH)_2$-CNTs (80 °C) is 22.6 mA cm^{-2}, which is 2.94- and 2.69-fold higher than β-$Ni(OH)_2$ + CNTs (80 °C, 7.7 mA cm^{-2}) and β-$Ni(OH)_2$-CNTs (20 °C, 8.4 mA cm^{-2}). The

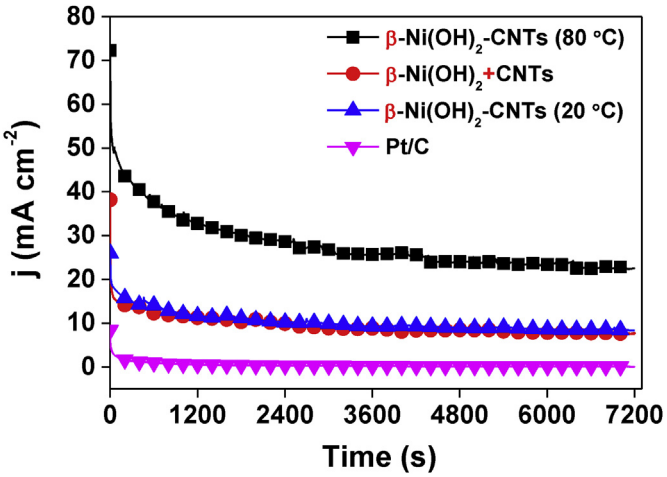

Fig. 7. Chronoamperometric curves of β-$Ni(OH)_2$-CNTs (80 °C), β-$Ni(OH)_2$+CNTs (mixture), β-$Ni(OH)_2$-CNTs (20 °C) and Pt/C (20 wt%) at a constant potential of 0.45 V (vs. SCE) running for 7200 s in 1.0 M KOH +0.33 M urea solution.

excellent electrocatalytic stability of β-$Ni(OH)_2$-CNTs (80 °C) for urea electro-oxidation is also proved by multi-cycles CV method (Fig. S9), where the β-$Ni(OH)_2$-CNTs (80 °C) catalyst also shows the smallest peak current density degradation after continuous 50 cycles of operation than these of the β-$Ni(OH)_2$+CNTs (80 °C), β-$Ni(OH)_2$-CNTs (20 °C) and Pt/C (20 wt%) catalysts in 1.0 M KOH + 0.33 M urea solution.

4. Conclusion

In summary, a series of β-$Ni(OH)_2$-CNTs catalysts has been synthesized by a facile hydrothermal method at different synthetic temperatures. The crystal structures, morphologies, and chemical states have been carefully characterized by various technologies. The results show that the lamellar structures of β-$Ni(OH)_2$-CNTs (80 °C) catalyst contains *ca.* 54.2% Ni(III) species in the hybrid catalyst. The electrochemical studies find that the β-$Ni(OH)_2$-CNTs (80 °C) catalyst exhibits the largest ESA value (95.6 $m^2 g^{-1}$), highest catalytic activity (98.5 mA cm^{-2}) and stability for urea electro-oxidation. The excellent performance of β-$Ni(OH)_2$-CNTs (80 °C) catalyst is mainly contributed to the unique lamellar structures, high content of Ni(III) species and uniform distributed of β-$Ni(OH)_2$ on CNTs support in the hybrid catalyst. Therefore, we strongly believe that the high performance catalyst and the fabrication methods have a great potential applications in the field of fuel cells, water splitting, lithium battery, *etc.*

Table 1
Comparison with various previous reported catalysts for urea electro-oxidation in 1.0 M KOH solution.

Catalyst	Onset potential (V)	Peak current (mA cm^{-2})	Electrolyte	Reference electrode
β-$Ni(OH)_2$-CNTs$^{(this\ work)}$	0.32	98.5	0.33 M urea	SCE
S-doped $Ni(OH)_2$ [29]	0.33	~37	0.33 M urea	Ag/AgCl
Ni_2Mo_1/G [50]	0.39	128	0.33 M urea	Ag/AgCl
NiO-Fe_2O_3/rGO [21]	0.32	44.6	0.33 M urea	Ag/AgCl
Nickel phosphate [51]	0.45	49	0.33 M urea	Ag/AgCl
$Ni_{1.5}Mn_{1.5}O_4$ [13]	0.29	6.9	0.33 M urea	Ag/AgCl
Nickel/graphene [19]	0.32	150	2.0 M urea	Ag/AgCl
α-$Ni(OH)_2$@CNT [28]	0.43	~50	0.33 M urea	Hg/HgO
$NiCo_2O_4$ [52]	0.45	136	0.33 M urea	Hg/HgO
Ni_2P NF/CC [53]	0.30	100	0.5 M urea	SCE
Ni-P [18]	1.37	70	0.33 M urea	RHE
Ni NP/NiFe LDH [54]	1.34	300	0.5 M urea	RHE
MnO_2/$MnCo_2O_4$/Ni [23]	1.33	384	0.5 M urea	RHE

Notes

The authors declare no competing financial interest.

Acknowledgements

This work has been supported by the National Natural Science Foundation of China (21163002, 21165004, 21363003), Natural Science Foundation of Guangxi Province (2014GXNSFFA118003, 2014GXNSFGA118008), BAGUI scholar program (2014A001), Project of Talents Highland of Guangxi Province and Guangxi Key Laboratory of Low Carbon Energy Materials.

Appendix A. Supplementary data

Supplementary data to this article can be found online at https://doi.org/10.1016/j.electacta.2019.01.150.

References

[1] G.W. Huber, J.W. Shabaker, J.A. Dumesic, Raney Ni-Sn catalyst for H_2 production from biomass-derived hydrocarbons, Science 300 (2003) 2075–2077.
[2] G. Wang, Y. Ling, X. Lu, H. Wang, F. Qian, Y. Tong, Y. Li, Solar driven hydrogen releasing from urea and human urine, Energy Environ. Sci. 5 (2012) 8215–8219.
[3] X. Yang, A.-Y. Lu, Y. Zhu, M.N. Hedhili, S. Min, K.-W. Huang, Y. Han, L.-J. Li, CoP nanosheet assembly grown on carbon cloth: a highly efficient electrocatalyst for hydrogen generation, Nanomater. Energy 15 (2015) 634–641.
[4] X. Yang, A.-Y. Lu, Y. Zhu, S. Min, M.N. Hedhili, Y. Han, K.-W. Huang, L.-J. Li, Rague-like FeP nanocrystal assembly on carbon cloth: an exceptionally efficient and stable cathode for hydrogen evolution, Nanoscale 7 (2015) 10974–10981.
[5] B.K. Boggs, R.L. King, G.G. Botte, Urea electrolysis: direct hydrogen production from urine, Chem. Commun. (2009) 4859–4861.
[6] A. Yousef, M.H. El-Newehy, S.S. Al-Deyab, N.A.M. Barakat, Facile synthesis of Ni-decorated multi-layers graphene sheets as effective anode for direct urea fuel cells, Arab, J. Chem. 10 (2017) 811–822.
[7] C. Li, Y. Liu, Z. Zhuo, H. Ju, D. Li, Y. Guo, X. Wu, H. Li, T. Zhai, Local charge distribution engineered by Schottky heterojunctions toward urea electrolysis, Adv. Energy Mater. 8 (2018), 1801775.
[8] R. Lan, S. Tao, J.T.S. Irvine, A direct urea fuel cell-power from fertiliser and waste, Energy Environ. Sci. 3 (2010) 438–441.
[9] H. Kuwayama, K. Itadani, T. Kameyama, S. Kuwabata, T. Torimoto, Improved electrocatalytic oxidation of urea using Ru-Ni binary nanoparticles prepared by an ionic liquid/metal sputtering technique, Meet. Abstr. (2016) 3474. MA2016-02.
[10] E. Urbańczyk, A. Jaroń, W. Simka, Electrocatalytic oxidation of urea on a sintered Ni–Pt electrode, J. Appl. Electrochem. 47 (2017) 133–138.
[11] W. Xu, D. Du, R. Lan, J. Humphreys, Z. Wu, S. Tao, Highly active Ni–Fe double hydroxides as anode catalysts for electrooxidation of urea, New J. Chem. 41 (2017) 4190–4196.
[12] F. Guo, K. Ye, M. Du, K. Cheng, Y. Gao, G. Wang, D. Cao, Nickel nanowire arrays electrode as an efficient catalyst for urea peroxide electro-oxidation in alkaline media, Electrochim. Acta 190 (2016) 150–158.
[13] S. Periyasamy, P. Subramanian, E. Levi, D. Aurbach, A. Gedanken, A. Schechter, Exceptionally active and stable spinel nickel manganese oxide electrocatalysts for urea oxidation reaction, ACS Appl. Mater. Interfaces 8 (2016) 12176–12185.
[14] Q. Liu, L. Xie, F. Qu, Z. Liu, G. Du, A.M. Asiri, X. Sun, A porous Ni_3N nanosheet array as a high-performance non-noble-metal catalyst for urea-assisted electrochemical hydrogen production, Inorg. Chem. Front. 4 (2017) 1120–1124.
[15] M.-S. Wu, C.-Y. Jao, F.-Y. Chuang, F.-Y. Chen, Carbon-encapsulated nickel-iron nanoparticles supported on nickel foam as a catalyst electrode for urea electrolysis, Electrochim. Acta 227 (2017) 210–216.
[16] S. Wei, X. Wang, J. Wang, X. Sun, L. Cui, W. Yang, Y. Zheng, J. Liu, CoS_2 nanoneedle array on Ti mesh: a stable and efficient bifunctional electrocatalyst for urea-assisted electrolytic hydrogen production, Electrochim. Acta 246 (2017) 776–782.
[17] N. Kakati, J. Maiti, K.S. Lee, B. Viswanathan, Y.S. Yoon, Hollow sodium nickel fluoride nanocubes deposited MWCNT as an efficient electrocatalyst for urea oxidation, Electrochim. Acta 240 (2017) 175–185.
[18] R. Ding, X. Li, W. Shi, Q. Xu, L. Wang, H. Jiang, Z. Yang, E. Liu, Mesoporous Ni-P nanocatalysts for alkaline urea electrooxidation, Electrochim. Acta 222 (2016) 455–462.
[19] N.A.M. Barakat, M. Motlak, Z.K. Ghouri, A.S. Yasin, M.H. El-Newehy, S.S. Al-Deyab, Nickel nanoparticles-decorated graphene as highly effective and stable electrocatalyst for urea electrooxidation, J. Mol. Catal. Chem. 421 (2016) 83–91.
[20] D. Wang, S.H. Vijapur, Y. Wang, G.G. Botte, $NiCo_2O_4$ nanosheets grown on current collectors as binder-free electrodes for hydrogen production via urea electrolysis, Int. J. Hydrogen Energy 42 (2017) 3987–3993.
[21] G. Das, R.M. Tesfaye, Y. Won, H.H. Yoon, NiO-Fe_2O_3 based graphene aerogel as urea electrooxidation catalyst, Electrochim. Acta 237 (2017) 171–176.
[22] X. Wang, J. Wang, X. Sun, S. Wei, L. Cui, W. Yang, J. Liu, Hierarchical coral-like NiMoS nanohybrids as highly efficient bifunctional electrocatalysts for overall urea electrolysis, Nano Res 11 (2018) 988–996.
[23] C. Xiao, S. Li, x. zhang, D. MacFarlane, MnO_2/$MnCo_2O_4$/Ni heterostructure with quadruple hierarchy: a bifunctional electrode architecture for overall urea oxidation, J. Mater. Chem. 5 (2017) 7825–7832.
[24] D. Zhu, C. Guo, J. Liu, L. Wang, Y. Du, S.Z. Qiao, Two-dimensional metal-organic frameworks with high oxidation states for efficient electrocatalytic urea oxidation, Chem. Commun. 53 (2017) 10906–10909.
[25] D. Wang, W. Yan, G.G. Botte, Exfoliated nickel hydroxide nanosheets for urea electrolysis, Electrochem. Commun. 13 (2011) 1135–1138.
[26] M.A. Ghanem, A.M. Al-Mayouf, J.P. Singh, P. Arunachalam, Concurrent deposition and exfoliation of nickel hydroxide nanoflakes using liquid crystal template and their activity for urea electrooxidation in alkaline medium, Electrocatalysis 8 (2017) 16–26.
[27] X. Zhang, G. Liu, C. Zhao, G. Wang, Y. Zhang, H. Zhang, H. Zhao, Highly efficient electrocatalytic oxidation of urea on a Mn-incorporated $Ni(OH)_2$/carbon fiber cloth for energy-saving rechargeable Zn-air batteries, Chem. Commun. 53 (2017) 10711–10714.
[28] L. Bian, T. Du, Q. Du, M. Luo, M. Li, Multiwalled carbon nanotubes twined α-nickel hydroxide microspheres as high-efficient urea electrooxidation catalysts, J. Appl. Electrochem. 47 (2017) 905–915.
[29] X. Zhu, X. Dou, J. Dai, X. An, Y. Guo, L. Zhang, S. Tao, J. Zhao, W. Chu, X.C. Zeng, C. Wu, Y. Xie, Metallic nickel hydroxide nanosheets give superior electrocatalytic oxidation of urea for fuel cells, Angew. Chem. Int. Ed. 55 (2016) 12465–12469.
[30] X. Yu, J. Zhao, L.-R. Zheng, Y. Tong, M. Zhang, G. Xu, C. Li, J. Ma, G. Shi, Hydrogen evolution reaction in alkaline media: alpha- or beta-nickel hydroxide on the surface of platinum? ACS Energy Lett 3 (2017) 237–244.
[31] X. Yang, H. Li, A.-Y. Lu, S. Min, Z. Idriss, M.N. Hedhili, K.-W. Huang, H. Idriss, L.-J. Li, Highly acid-durable carbon coated Co_3O_4 nanoarrays as efficient oxygen evolution electrocatalysts, Nanomater. Energy 25 (2016) 42–50.
[32] Y. Zhao, X. Yang, L. Zhan, S. Ou, J. Tian, High electrocatalytic activity of PtRu nanoparticles supported on starch-functionalized multi-walled carbon nanotubes for ethanol oxidation, J. Mater. Chem. 21 (2011) 4257–4263.
[33] J. Zhang, X. Yang, H. Shao, C.-C. Tseng, S. Tian, W. Hu, C. Jing, J. Tian, Y. Zhao, Microwave-Assisted synthesis of Pd oxide-rich Pd particles on nitrogen/sulfur Co-doped graphene with remarkably enhanced ethanol electrooxidation, Fuel Cells 17 (2017) 115–122.
[34] X. Yang, X. Liu, X. Meng, X. Wang, G. Li, C. Shu, L. Jiang, C. Wang, Self-assembly of highly dispersed Pt and PtRu nanoparticles on perylene diimide derivatives functionalized carbon nanotubes as enhanced catalysts for methanol electrooxidation, J. Power Sources 240 (2013) 536–543.
[35] Y.-J. Shih, Y.-H. Huang, C.P. Huang, Electrocatalytic ammonia oxidation over a nickel foam electrode: role of $Ni(OH)_2$(s)-NiOOH(s) nanocatalysts, Electrochim. Acta 263 (2018) 261–271.
[36] C. Lin, Z. Gao, F. Zhang, J. Yang, B. Liu, J. Jin, In-situ growth of single-layered α-$Ni(OH)_2$ nanosheets on carbon cloth for high-efficient electrocatalytic urea oxidation, J. Mater. Chem. 6 (2018) 13867–13873.
[37] Y. Zhao, X. Yang, J. Tian, Electrocatalytic oxidation of methanol at 2-aminophenoxazin-3-one-functionalized multiwalled carbon nanotubes supported PtRu nanoparticles, Electrochim. Acta 54 (2009) 7114–7120.
[38] X. Peng, D. Chen, X. Yang, D. Wang, M. Li, C.-C. Tseng, R. Panneerselvam, X. Wang, W. Hu, J. Tian, Y. Zhao, Microwave-Assisted synthesis of highly dispersed PtCu nanoparticles on three-dimensional nitrogen-doped graphene networks with remarkably enhanced methanol electrooxidation, ACS Appl. Mater. Interfaces 8 (2016) 33673–33680.
[39] G.-X. Tong, F.-T. Liu, W.-H. Wu, J.-P. Shen, X. Hu, Y. Liang, Polymorphous α- and β-$Ni(OH)_2$ complex architectures: morphological and phasal evolution mechanisms and enhanced catalytic activity as non-enzymatic glucose sensors, CrystEngComm 14 (2012) 5963–5973.
[40] T. Tang, Q. Gan, X. Guo, H. Dong, J. Zhang, Y. Zhao, J. Tian, X. Yang, A hybrid catalyst of Pt/$CoNiO_2$ on carbon nanotubes and its synergetic effect towards remarkable ethanol electro-oxidation in alkaline media, Sustain. Energ. Fuels 2 (2018) 229–236.
[41] D.S. Hall, D.J. Lockwood, C. Bock, B.R. MacDougall, Nickel hydroxides and related materials: a review of their structures, synthesis and properties, Proc. R. Soc. A-Math. Phys. Eng. Sci. 471 (2015) 20140792.
[42] M.C. Bernard, R. Cortes, M. Keddam, H. Takenouti, P. Bernard, S. Senyarich, Structural defects and electrochemical reactivity of β-$Ni(OH)_2$, J. Power Sources 63 (1996) 247–254.
[43] C. Wu, J. Zhang, J. Guo, L. Sun, J. Ming, H. Dong, Y. Zhao, J. Tian, X. Yang, Ceria-induced strategy to tailor Pt atomic clusters on cobalt–nickel oxide and the synergetic effect for superior hydrogen generation, ACS Sustain. Chem. Eng. 6 (2018) 7451–7457.
[44] L. Zhu, T. Zheng, J. Zheng, C. Yu, N. Zhang, Q. Zhou, W. Zhang, B.H. Chen, Shape control of nickel crystals and catalytic hydrogenation performance of ruthenium-on-Ni crystals, CrystEngComm 20 (2018) 113–121.
[45] B.M. Jović, U.Č. Lačnjevac, V.D. Jović, L. Gajić-Krstajić, J. Kovač, D. Poleti, N.V. Krstajić, Ni-(Ebonex-supported Ir) composite coatings as electrocatalysts

for alkaline water electrolysis. Part II: oxygen evolution, Int. J. Hydrogen Energy 41 (2016) 20502–20514.
[46] J. Sun, N. Guo, Z. Shao, K. Huang, Y. Li, F. He, Q. Wang, A facile strategy to construct amorphous spinel-based electrocatalysts with massive oxygen vacancies using ionic liquid dopant, Adv. Energy Mater. 0 (2018), 1800980.
[47] S. Gao, F. Liao, S. Ma, L. Zhu, M. Shao, Network-like mesoporous $NiCo_2O_4$ grown on carbon cloth for high-performance pseudocapacitors, J. Mater. Chem. 3 (2015) 16520–16527.
[48] Y. Tong, P. Chen, M. Zhang, T. Zhou, L. Zhang, W. Chu, C. Wu, Y. Xie, Oxygen vacancies confined in nickel molybdenum oxide porous nanosheets for promoted electrocatalytic urea oxidation, ACS Catal. 8 (2018) 1–7.
[49] D.A. Daramola, D. Singh, G.G. Botte, Dissociation rates of urea in the presence of NiOOH catalyst: a DFT analysis, J. Phys. Chem. 114 (2010) 11513–11521.
[50] W. Shi, R. Ding, X. Li, Q. Xu, E. Liu, Enhanced performance and electrocatalytic kinetics of Ni-Mo/graphene nanocatalysts towards alkaline urea oxidation reaction, Electrochim. Acta 242 (2017) 247–259.
[51] M.A. Al-Omair, A.H. Touny, M.M. Saleh, Reflux-based synthesis and electrocatalytic characteristics of nickel phosphate nanoparticles, J. Power Sources 342 (2017) 1032–1039.
[52] R. Ding, L. Qi, M. Jia, H. Wang, Facile synthesis of mesoporous spinel $NiCo_2O_4$ nanostructures as highly efficient electrocatalysts for urea electro-oxidation, Nanoscale 6 (2014) 1369–1376.
[53] D. Liu, T. Liu, L. Zhang, F. Qu, G. Du, A.M. Asiri, X. Sun, High-performance urea electrolysis towards less energy-intensive electrochemical hydrogen production using a bifunctional catalyst electrode, J. Mater. Chem. 5 (2017) 3208–3213.
[54] X. Gao, X. Long, H. Yu, X. Pan, Z. Yi, Ni nanoparticles decorated NiFe layered double hydroxide as bifunctional electrochemical catalyst, J. Electrochem. Soc. 164 (2017) H307–H310.
[55] M. Jafarian, F. Forouzandeh, I. Danaee, F. Gobal, M.G. Mahjani, Electrocatalytic oxidation of glucose on Ni and NiCu alloy modified glassy carbon electrode, J. Solid State Electrochem. 13 (2009) 1171–1179.